China Ocean Eng., Vol. 28, No. 5, pp. 701 – 712

DOI 10.1007/s13344-014-0054-z, ISSN 0890-5487

Numerical Simulation of Breaking Wave Generated Sediment Suspension and Transport Process Based on CLSVOF Algorithm*

LU Xin-hua (卢新华)[a, b, 1], ZHANG Xiao-feng (张小峰)[a],

LU Jun-qing (陆俊卿)[c, d] and DONG Bing-jiang (董炳江)[e]

[a] *State Key Laboratory of Water Resources and Hydropower Engineering Science*, *Wuhan University*, *Wuhan 430072*, *China*

[b] *State Key Laboratory of Hydrology-Water Resources and Hydraulic Engineering*, *Hohai University*, *Nanjing 210098*, *China*

[c] *State Key Laboratory of Simulation and Regulation of Water Cycle in River Basin*, *China Institute of Water Resources and Hydropower Research*, *Beijing 100044*, *China*

[d] *South China Institute of Environmental Science*, *Ministry of Environmental Protection*, *Guangzhou 510655*, *China*

[e] *Hydrology Bureau*, *Yangtze River Water Resource Commission*, *Wuhan 430010*, *China*

(Received 15 November 2012; received revised form 17 October 2013; accepted 16 January 2014)

ABSTRACT

The sediment suspension and transport process under complex breaking wave situation is investigated using large eddy simulation (abbreviated as LES hereafter) method. The coupled level set (LS) and volume of fluid (VOF) method is used to accurately capture the evolution of air−water interface. The wall effect at the bottom is modeled based on the wave friction term while the complicate bottom boundary condition for sediment is tackled using Chou and Fringer's sediment erosion and deposition flux method. A simulation is carried out to study the sediment suspension and transport process under periodic plunging breaking waves. The comparison between the results by CLSVOF method and those obtained by the LS method is given. It shows that the latter performs as well as the CLSVOF method in the pre-breaking weak-surface deformation situation. However, a serious mass conservation problem in the later stages of wave breaking makes it inappropriate for this study by use of the LS method and thus the CLSVOF method is suggested. The flow field and the distribution of suspended sediment concentration are then analyzed in detail. At the early stage of breaking, the sediment is mainly concentrated near the bottom area. During the wave breaking process, when the entrapped large-scale air bubble travels downward to approach the bottom, strong shear is induced and the sediment is highly entrained.

Key words: *sediment suspension*; *wave breaking*; *subgrid-scale model*; *CLSVOF*; *level set*

1. Introduction

It is well known that fluid–sediment interactions in the near-shore coastal region can lead to

* This work was financially supported by the National Natural Science Foundation of China (Grant Nos. 51409195 and 51379155), the Open Foundation of State Key Laboratory of Hydrology-Water Resources and Hydraulic Engineering (Grant No. 2013491111), the China Postdoctoral Science Foundation (Grant No. 2014M550408), the Fundamental Research Funds for the Central Universities (Grant No. 2042014kf0068), and the Open Research Fund of State Key Laboratory of Simulation and Regulation of Water Cycle in River Basin (China Institute of Water Resources and Hydropower Research, Grant No. IWHR-SKL-201112).

1 Corresponding author. E-mail: xhluhh@whu.edu.cn

significant seabed erosion and deposition processes. It causes lots of engineering problems, such as decrease of navigation depth due to sedimentation, and beach erosion by scouring. In these processes, the powerful breaking waves play an important role in for example, entraining sediment into suspension, generating turbulence which mixes the sediment and other materials (Bai and Ng, 2002; Cao and Wang, 1993).

Many studies have been carried out to study the sediment suspension and transport mechanism in the hydrodynamic complicated ocean environment. However, it is still difficult to predict the suspension and transport processes either by experiment study or numerical modeling (theoretical analysis is impossible). Observations in the field and experiment are difficult since wave breaking is a strongly nonlinear intermittent process and during which different scales of air bubbles are entrapped (Melville, 1996; Lakehal and Liovic, 2011; Kiger and Duncan, 2012).

In the concern of mathematical simulation, currently the only practical method for this study is the wall-modeled LES (Zeldler and Street, 2001; Chou and Fringer, 2008) or wall-modeled RANS (Reynolds-averaged Navier–Stokes equations, Zeng *et al*., 2008; Wu *et al*., 2000). Since LES can directly resolve the large scale structures which are important for sediment suspension and transport, and the subgrid-scale model is more unified compared with Reynolds-stress closure model (Zhang *et al*., 2005), wall-modeled LES is an attractive tool for the sediment suspension and transport studies. Up till now, LES-based sediment simulation has been still challenged and limited. Zedler and Street (2001, 2006) simulated the sediment transport over sand ripples under both current and oscillatory flows with free-surface variation being neglected. The sediment suspension and deposition processes on sand ripples are qualitatively reproduced. However, the bottom boundary condition highly relies on the bottom turbulent diffusion coefficient, thus when the eddy viscosity is small near the bed, the results may be physically untrue. In view of this, Chou and Fringer proposed a physically-based bottom boundary condition for sediment transport (Chou and Fringer, 2008, 2010). In this method, van Rijn's sediment pick-up function (van Rijn, 1984) is used to account for all the subgrid-scale contributions. Bai and Ng (2002) tries to use LES in the investigation of sediment movement under plunging breaking waves. The flow field is studied. However, it is a pity that the free-surface boundary condition is simplified by using a zero-stress condition. Namely, the effect of air flow is neglected. This simplification may causes serious loss of accuracy since the water region may transfer as much as 50% of its initial energy to the air flows during wave breaking process (Iafrati, 2009; Hu *et al*., 2012).

As analyzed above, the tracking of strong time-varied air−water interface is one of the intractable issues for numerical study on sediment movement under breaking waves. During the past decades, a number of different methods have been developed for complex two-phase flow simulations, among which the VOF and LS methods are mostly used nowadays. The VOF method is proposed by Hirt and Nichols (1981). With this method, a convection equation is solved for the volume fraction function in each control volume. Since the integration of the volume fraction in the whole domain represents the mass of water, accurate mass conservation can be achieved. However, since the spatial derivatives of the volume fraction function are not continuous near the interface, it is difficult to accurately calculate the interface normal or curvature (Hirt and Nichols, 1981; Sun and Tao, 2010). On the contrary, this difficulty has been well overcomed by use of the LS method proposed by Sussman *et al*. (1994). In this method, a

smoothly signed distance function is defined, which denotes the signed and minimal distance to the interface. The LS method cannot ensure mass conservation (Sussman, 2000; Sussman and Puckett, 2003; Sun and Tao, 2010). To overcome the demerits in both of the LS method and VOF method, the CLSVOF algorithm is introduced by Bourlioux (1995) and later well developed by Sussmann (2000) and Sussman and Puckett (2003). This method reconstructs the interface from VOF functions to ensure the mass conservation, while calculates the interface normal and curvature based on LS functions.

In this paper, different interface tracking methods (LS and CLSVOF) are used and the results from them are compared. The wave breaking process and the sediment movement under plunging breaking waves are studied.

2. Numerical Model

2.1 Governing Equations

The governing equations for air−water two-phase flow (vertical 2D) can be described by the filtered Navier-Stokes equations:

flow momentum equation

$$\frac{\partial \boldsymbol{u}}{\partial t}+\nabla\cdot(\boldsymbol{u}\cdot\boldsymbol{u})=-\frac{1}{\rho}\nabla\prod+\frac{\mu}{\rho}\nabla\cdot(2\bar{D})-g\,\boldsymbol{j}-\frac{1}{\rho}\gamma\kappa\delta(\phi)\nabla\phi-\boldsymbol{F}, \tag{1}$$

and flow continuity equation

$$\nabla\cdot\boldsymbol{u}=0, \tag{2}$$

where, $\boldsymbol{u}=(u,v)$ is the flow vector and u and v are the flow components in the streamwise x and the vertical y direction, respectively; t denotes the time; $\prod=P_{\mathrm{d}}+P_{\mathrm{h}}$ is the total pressure, where $P_{\mathrm{h}}=-\int_y\rho g\mathrm{d}y$ and P_{d} is the dynamic pressure; $\bar{D}_{ij}=(\partial u_i/\partial x_j+\partial u_j/\partial x_i)/2$ is the deformation tensor; g is the acceleration due to gravity and $\boldsymbol{j}$ is the unit vector in the vertical direction; γ is the surface tension coefficient; $F_i=\partial\tau_{ij}/\partial x_j=\partial(\overline{u_iu_j}-\bar{u}_i\bar{u}_j)/\partial x_j$ is the subgrid-scale term to represent the effect caused by the unresolved subgrid-scale motions; $\delta(\phi)=\mathrm{d}H(\phi;\varepsilon)/\mathrm{d}\phi$, where $H(\phi;\varepsilon)$ is Heaviside function; ϕ is the LS distance function which is positive in the water and negative in the air; ε is the interface smoothing thickness; $\kappa=-\nabla\cdot(\nabla\phi/|\nabla\phi|)$ is the interface curvature; ρ and μ denote flow density and dynamic viscosity expressed respectively as:

$$\rho(\phi)=\rho_{\mathrm{a}}+(\rho_{\mathrm{w}}-\rho_{\mathrm{a}})\cdot H(\phi;\varepsilon); \tag{3}$$

$$\mu(\phi)=\mu_{\mathrm{a}}+(\mu_{\mathrm{w}}-\mu_{\mathrm{a}})\cdot H(\phi;\varepsilon), \tag{4}$$

where, the subscripts “w” and “a” denote water and air, respectively.

In this study, the following function of $H(\phi;\varepsilon)$ is used

$$H(\phi;\varepsilon)=\begin{cases}1 & \phi>\varepsilon\\ \dfrac{1}{2}\left[1+\dfrac{\phi}{\varepsilon}+\dfrac{1}{\pi}\sin\left(\dfrac{\phi\pi}{\varepsilon}\right)\right] & |\phi|\le\varepsilon\\ 0 & \text{else}\end{cases} \tag{5}$$

To model the subgrid-scale stress, the subgrid-scale model based on the renormalization group theory (abbreviated as RNG-LES hereafter) is adopted (Yakhot and Orszag, 1986). This is a theoretical model that has no tunable coefficients and besides, reasonable subgrid-scale viscosity near the wall is predicted. Besides, RNG-LES model has the self-adaption capability of switching from laminar flow to turbulent flow regime, thus it is appropriate for this study since physically no- or low-turbulence is generated in the pre-breaking stage.

In the RNG-LES model, the subgrid-scale stress is modeled as:

$$\tau_{ij}-\frac{1}{3}\tau_{kk}\delta_{ij}=-2\nu_{\text{sgs}}\overline{D}_{ij}\,; \tag{6}$$

and ν_{sgs} is calculated from

$$\nu_{\text{sgs}}+\nu=\nu\left[1+H\left(\frac{\nu_{\text{s}}^2\cdot(\nu_{\text{sgs}}+\nu)}{\nu^3}-C\right)\right]^{1/3}, \tag{7}$$

where, $\nu_{\text{s}}=C_{\text{RNG}}\Delta^2\sqrt{2\overline{D}_{ij}\,\overline{D}_{ij}}$; function H is expressed as:

$$H(x)=\begin{cases}x & x>0\\ 0 & \text{else}\end{cases} \tag{8}$$

The coefficients $C=75$ and $C_{\text{RNG}}=0.0062$ are theoretically obtained through renormalization group theory (Yakhot and Orszag, 1986).

The governing equation for sediment transport is a convection-diffusion equation expressed as:

$$\frac{\partial s}{\partial t}+\frac{\partial(u_i-\omega_{\text{s}}\delta_{i2})s}{\partial x_i}=\frac{\partial s}{\partial x_i}\left(\frac{\nu+\nu_{\text{sgs}}}{Sc_{\text{t}}}\frac{\partial s}{\partial x_i}\right), \tag{9}$$

where, s is the suspended sediment concentration in volume; ω_{s} is the sediment settling velocity; δ is the Kronecker operator; Sc_{t} is the Schmidt number and is chosen as 1.2 in this paper.

2.2 LS Free-Surface Tracking Method

In the framework of LS method, a signed distance function ϕ is defined. The physical meaning of ϕ is the signed and shortest normal distance from interface. Therefore, the interface is represented by the zero-isosurface of ϕ. The evolution of ϕ is governed by

$$\frac{\partial\phi}{\partial t}+\boldsymbol{u}\cdot\nabla\phi=0\,. \tag{10}$$

Eq. (10) can be easily solved since ϕ is a smooth function even near the interface. However, as is known that ϕ cannot maintain as a distance function after some simulation time. This problem is avoided by use of the reinitilization technique. In this method, the following equation is solved to a steady state

$$\frac{\partial\phi}{\partial\tau}=\frac{\phi_0}{\sqrt{\phi_0^2+\varepsilon_{\text{d}}^2}}(1-|\nabla\phi|)\,, \tag{11}$$

where, ϕ_0 corresponds to the value at the last time step; τ is a virtual time for iteration; ε_d is a small positive value taken as 10^{-6} in this paper to avoid zero denominator.

2.3 Implementation of the CLSVOF Algorithm

In the framework of VOF method, the following governing equation is solved

$$\frac{\partial F}{\partial t}+\nabla\cdot(\boldsymbol{u}F)=0\,, \tag{12}$$

where, F is the volume function.

A second order operator split algorithm is used for the discretizations of Eqs. (10) and (12). The discretization is based on a staggered grid as illustrated in Fig. 1.

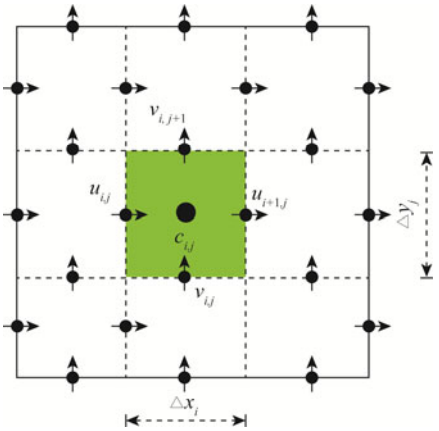

Fig. 1. Layout of variables on a staggered grid.

Given the LS distance function ϕ^0 and the VOF volume fraction F^0 at the last time step, for a general scalar c, the conservative operator split advection scheme is implemented as follows:

$$c_{i,j}^1=\frac{c_{i,j}^0+(\Delta t/\Delta x_i)(G_{i,j}^1-G_{i+1,j}^1)}{1-(\Delta t/\Delta x_i)(u_{i+1,j}-u_{i,j})}\,; \tag{13}$$

$$c_{i,j}^2=\frac{c_{i,j}^1+(\Delta t/\Delta y_j)(G_{i,j}^2-G_{i,j+1}^2)}{1-(\Delta t/\Delta y_j)(v_{i,j+1}-v_{i,j})}\,; \tag{14}$$

$$c_{i,j}^{n+1}=c_{i,j}^0-\Delta t\left[\frac{c_{i,j}^1}{\Delta x_i}(u_{i+1,j}-u_{i,j})+\frac{c_{i,j}^2}{\Delta y_j}(v_{i,j+1}-v_{i,j})\right], \tag{15}$$

where, $G_{i,j}^1=u_{i,j}c_{i-1/2,j}$ and $G_{i,j}^2=v_{i,j}c_{i,j-1/2}$ denote the fluxes across the control volume faces. The above algorithm is of the second order accurate when the alternating sweep direction method is used at each time step.

The complete algorithm for the CLSVOF method is illustrated in Fig. 2.

2.4 Bottom Boundary Condition for Flow and Sediment

As the staggered grid is used for discretization, the first streamwise velocity point is half grid away from the bed. The bottom friction velocity u_* is calculated from

$$u_* = \sqrt{\frac{f_w}{2}} \, | u_b | , \tag{16}$$

where, u_b is the velocity parallel to the bed at the first streamwise velocity point, and f_w is the wave friction coefficient (Nielsen, 1992) calculated as:

$$f_w = \exp\left[5.5\left(\frac{k_s}{A}\right)^{0.2} - 6.3 \right], \tag{17}$$

where, $k_s = 2d_{50}$ and $A = a / \sinh(2\pi h_w / \lambda)$. Here, d_{50} denotes the sediment particle diameter; a is the wave amplitude; h_w denotes water depth and λ is the wave length.

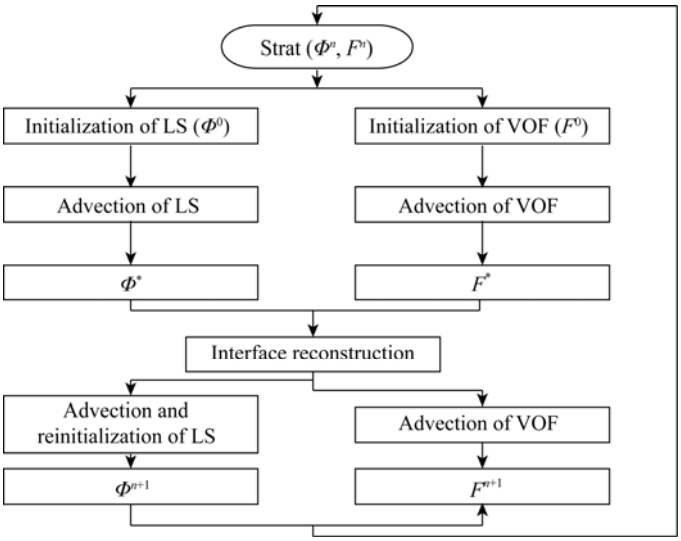

Fig. 2. Sketch of the CLSVOF algorithm.

The shear stress at the bottom is calculated from Eq. (16) and then served as boundary condition for flow simulation and also used to calculate Shields parameter in the sediment erosion flux described below.

The nearbed sediment erosion flux E and deposition flux D is calculated respectively from

$$E(t) = p_k(t) = \begin{cases} 0.00033\left(\dfrac{\theta(t)-\theta_c}{\theta_c}\right)^{1.5} \dfrac{(\rho_s/\rho_w - 1)^{0.6} g^{0.6} d_{50}^{0.8}}{\nu_w^{0.2}}, & \theta(t) > \theta_c \\ 0, & \text{else} \end{cases} \tag{18}$$

$$D(t) = \omega_s s_{bed} \tag{19}$$

where, $p_k(t)$ is the sediment pick-up function and $\theta(t)$ is the instantaneous Shields parameter calculated from

$$\theta(t) = \frac{u_*^2}{(\rho_s/\rho_w - 1) g d_{50}} . \tag{20}$$

In the above equations, θ_c is the critical Shields parameter; ρ_s denotes the density of sediment; ν_w is the kinematic viscosity of water; s_{bed} is the interpolated instantaneous suspended sediment concentration near the bed (Chou and Fringer, 2008, 2010).

2.5 Problem Definition and Solution Method

As a preliminary study, a 2D periodic wave propagating on a flat seabed is studied. The sketch of the studied problem is shown in Fig. 3. The setup of periodic 2D breaking wave is widely used in the previous literatures (Chen *et al*., 1999; Iafrati, 2009) since no additional treatment is needed to tackle the complex inlet and outlet reflections.

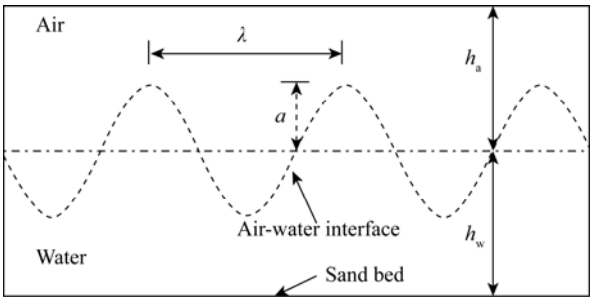

Fig. 3. Schematics of the studied problem.

The governing equation for flow is discretized by using the finite difference scheme. The essentially non-oscillatory scheme is used for spatial discretization. For the sediment transport equation, the HLPA scheme (Zhu, 1991; Icardi *et al*., 2011) is employed to discretize the convection term to resolve the strong concentration gradient. The second-order Runge−Kutta scheme is used for time integration. The divergence-free velocity field is obtained by using the projection method (Kim and Moin, 1985). MPI (Message Passing Interface) is used for parallelization. In the simulation, periodic boundary condition is imposed in the horizontal direction, and shear-free condition is imposed on the top boundary.

Owing to the small time scale in the simulation, seabed deformation is neglected (Bai and Ng, 2002; Chou and Fringer, 2008). The modeling of bed deformation requires implementation of complex boundary treatment method. One solution is to use the immersed boundary method (Mittal and Iaccarino, 2005), which will be incorporated into the current model in future to study the coupled flow-sediment-bed deformation problem.

3. Simulation Case and Results

In this simulation, the depth for water and air is chosen as $h_w = 0.1$ m and $h_a = 0.24$ m. The large air layer depth is used to capture all the potential air bubbles in the wave breaking process. The wavelength λ and wave period T is chosen as 1.4 m and 1.46 s, respectively. The initial wave slope $2\pi a/\lambda$ is set to 0.25. Theoretical analysis shows that wave breaks when the breaking index

$\gamma_b \approx 2a/h_w$ exceeds 0.78 (Zhou and Yan, 2009) and in our simulation $\gamma_b = 1.11$. Therefore, as the wave propagates, the wave profile becomes unstable and breaks.

The sediment particle diameter and density is chosen according to the generally practical situations in the ocean environment as $d_{50} = 0.0001$ m and $\rho_s = 2650$ kg/m^3.

The initial condition for flow is obtained from linear theory which is widely adopted to generate breaking waves (Lubin *et al*., 2006; Hu *et al*., 2012). Initially the suspended sediment concentration is set to zero. To ensure a grid-independent solution, a grid convergence study is carried out with four different spatial resolutions, namely, 100×90, 200×180, 400×180, and 400×360 with a time step $\Delta t = 0.00008$ s. The predicted near-bed suspended sediment concentration (horizontally-averaged) is shown in Fig. 4. It shows that the difference between the results from a 400×180 grid and a 400×360 grid is small, and we use a 400×180 grid in the following analysis.

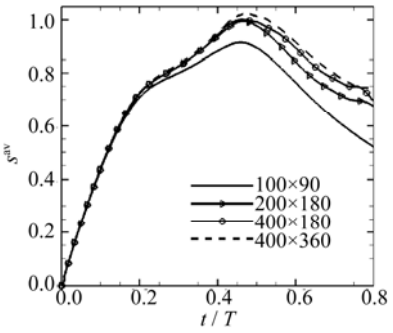

Fig. 4. Time history of the horizontally-averaged near-bed suspended sediment concentration with different spatial resolutions. Results are normalized by s^{av}_{max}, the maximum value during the simulation for the grid resolution 400×180.

3.1 Instantaneous Field of Flow and Sediment

A series of instantaneous velocity field and the distribution of suspended sediment concentration are illustrated in Fig. 5. The results obtained by use of the CLSVOF and pure LS method are shown.

In the pre-breaking stage (Fig. 5a), a jet is gradually formed around the wave crest, and then propagates forward. During this stage, the air−water interface has become asymmetric and an overturning motion has occurred. It is seen that the sediment is mainly concentrated near the bottom. After that the jet impacts the forward air−water interface, and then successive splash-up cycles are observed (Fig. 5b). In this stage, the air is entrained into the water and the bottom-accumulated sediment is transported upward. One may note that the velocity gradient near the air−water interface is larger in the air-side than that in the water part. This is consistent with the results in previous studies (Chen *et al*., 1999; Iafrati, 2009; Iafrati *et al*., 2001). The reason is that the shear stress is continuous at the air−water interface, and due to a rather small viscosity in the air region, and the velocity gradient is larger in the air phase.

Later on, the air bubbles either travel forward and down to approach the bottom or collapse and fragment into smaller air bubbles (Fig. 5c). When the large-scale air bubble approaches the bottom, strong shear flow is induced and the sediment is strongly entrained. The air bubbles are pushed back to the air−water interface by buoyancy and the local water velocity (Fig. 5d). In this stage, the sediment

has been distributed over the whole water depth due to the local flow field and the generated turbulence.

The comparison between the results obtained by CLSVOF and LS methods shows that the difference is negligible in the pre-breaking stage when the surface deformation is weak (Figs. 5a and 5e). During the strong breaking process (i.e. at $t = 0.47T$ and $t = 0.77T$), the significant mass conservation problem has occurred by using the LS method. As seen from Figs. 5f and 5g, different scales of air bubbles disappear. In the post-breaking process when turbulence is generated, the suspended sediment concentration field is similar between Fig. 5d and Fig. 5h with a more uniform distribution by use of the LS method.

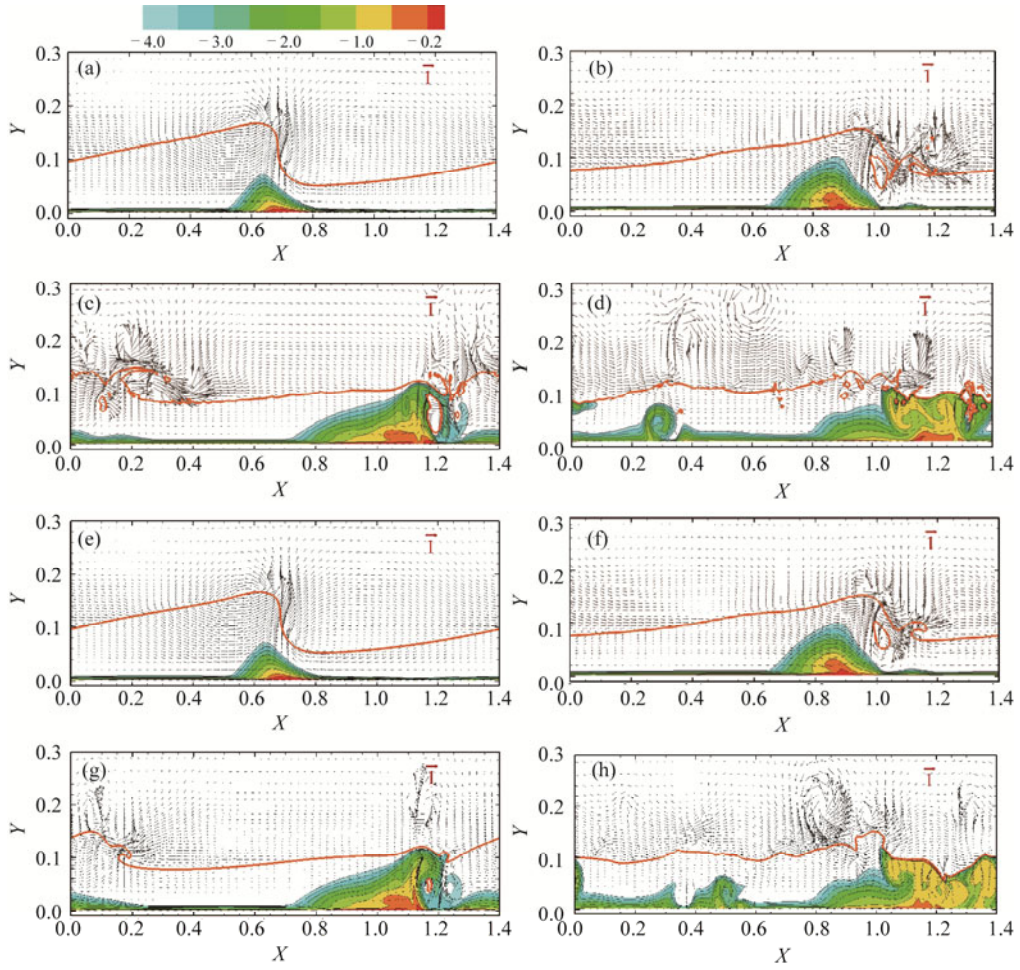

Fig. 5. Instantaneous flow field and the distribution of suspended sediment concentration at $t = 0.25T$, $t = 0.47T$, $t = 0.77T$, and $t = 1.30T$. (a)−(d) are the results from CLSVOF algorithm, while (e)−(f) are obtained from LS method. The orange-colored solid line represents the air−water interface. For a clear view consideration, the suspended sediment concentration is shown in a logarithmic scale ($\log_{10} s$). The suspended sediment concentration and velocity is normalized by $s_{\max}^{\mathrm{av}}$ and wave celerity c, respectively.

3.2 Statistics of Suspended Sediment Concentration and Sediment Fluxes

In Fig. 6a, the time history of total sediment in the domain $\sum s$ is illustrated. Here, $\sum s = \sum s_{i,j} \mathrm{d}x_i \mathrm{d}y_j$. In Fig. 6b, the horizontally-averaged nearbed sediment erosion flux E^{av} and deposition flux D^{av} are shown.

In the pre-breaking stage, the energy dissipates slowly. The friction velocity is large due to high bottom velocity (Fig. 5a). This causes large sediment erosion flux (Fig. 6b). Since the suspended sediment concentration is initially set to zero, no sediment deposits onto the bed at $t = 0$ (Fig. 6b). The difference between the high erosion flux and deposition flux causes the dramatic increase of sediment in the water domain (Fig. 6a). In this stage, the sediment is mainly concentrated around the bottom, thus the nearbed-averaged suspended sediment concentration goes up significantly (Fig. 5a). With the increase of nearbed suspended sediment concentration, the deposition flux rises quickly as shown in Fig. 6b.

During $t = 0.40 - 0.50T$, the energy has been highly dissipated after the onset of wave breaking and due to the bottom friction effect, the erosion flux at the bottom drops to approximately half of its peak value. It causes a low increasing rate of the total sediment in the whole domain in this period (Fig. 6a). When the erosion flux drops to lower than the deposition flux ($t > 5.0T$), the sediment in the whole water domain decreases as shown in Fig. 6a.

The above process continues until around $t = 0.75T$ the large-scale air bubble approaches the bottom as shown in Fig. 5c. This air bubble causes strong high-shear at the bottom and the erosion flux thus increases again to exceed the deposition flux (Fig. 6b). The sediment in the water domain then reaches the second peak around $t = 0.79T$. After that, as the air bubbles being brought up to the air–water interface and due to the higher energy dissipation (Iafrati, 2009; Hu, 2012), the bottom flow becomes weak (Fig. 5d) and the sediment in the domain gradually deposits to the bottom as shown in Fig. 6a.

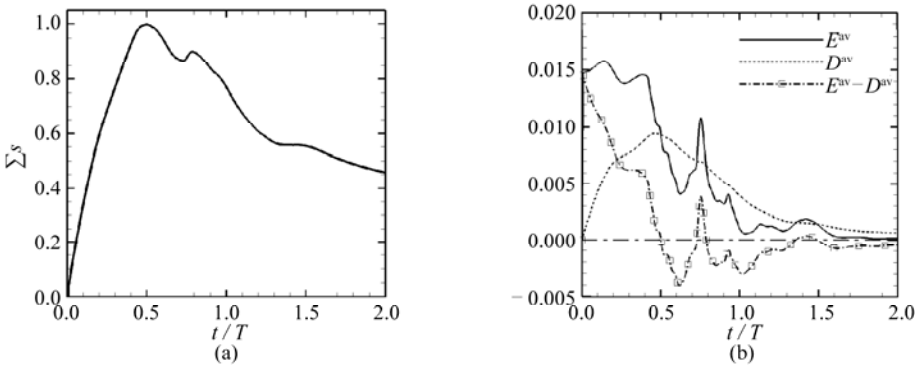

Fig. 6. Time history of $\sum s$ (a), and the horizontally-averaged sediment erosion and deposition flux at the bottom (b). The value of $\sum s$ and the erosion/deposition flux is normalized by $\lambda^2 \cdot s_{\max}^{\mathrm{av}}$ and $c \cdot s_{\max}^{\mathrm{av}}$, respectively.

4. Discussion and Conclusion

In this paper, the sediment suspension and transport process under plunging breaking wave

situation is studied by using the large eddy simulation method. The CLSVOF method is implemented to capture the air−water interface.

Results show that the CLSVOF algorithm performs well in tracking of the different scales of air bubbles during the wave breaking process, while the LS method shows serious mass conservation problem. Since the air bubbles are of great importance in this study, the CLSVOF method is suggested in future studies on sediment suspension under breaking waves. The results show that the sediment is mainly concentrated in a thin layer near the bed in the pre-breaking stage. When the large-scale air bubble moves to the seabed, strong shear is induced and serious erosion occurs.

Acknowledgements − The first author thanks Dr. X. Guo and Professor L. Shen for valuable discussions on this research.

References

Bai, Y. C. and Ng, C. O., 2002. Large eddy simulation for plunge breaker and sediment suspension, *China Ocean Eng*., **16**(2): 151−164.

Bourlioux, A., 1995. A coupled level-set volume-of-fluid algorithm for tracking material interfaces, *Proc. 6th Int. Symp. Comput. Fluid Dynam*., Lake Tahoe, CA, 15−22.

Cao, Z. D. and Wang, G. F., 1993. Numerical simulation of sediment lifted by wave and transported by tidal current, *Acta Oceanologica Sinica*, **15**(1): 107−118. (in Chinese)

Chen, G., Kharif, C., Zaleski, S. and Li, J., 1999. Two-dimensional Navier-Stokes simulation of breaking waves, *Phys. Fluids*, **11**(1): 121−133.

Chou, Y. J. and Fringer, O. B., 2008. Modeling dilute sediment suspension using large-eddy simulation with a dynamic mixed model, *Phys. Fluids*, **20**(11): 115103.

Chou, Y. J. and Fringer, O. B., 2010. A model for the simulation of coupled flow-bed form evolution in turbulent flows, *J. Geophys. Res*., **115**(C10): 1−20.

Hirt, C. W. and Nichols, B. D., 1981. Volume of fluid (VOF) method for the dynamics of free boundaries, *J. Comput. Phys*., **39**(1): 201−225.

Hu, Y., Guo, X., Lu. X. H., Liu, Y., Dalrymple, K. A. and Shen, L., 2012. Idealized numerical simulation of breaking water wave propagating over a viscous mud layer, *Phys. Fluids*, **24**(11): 112104.

Iafrati, A., 2009. Numerical study of the effects of the breaking intensity on wave breaking flows, *J. Fluid Mech*., **622**, 371−411.

Iafrati, A., Di Mascio, A. and Campana, E. F., 2001. A level set technique applied to unsteady free surface flows, *Int. J. Numer. Meth. Fluid*., **35**(3): 281−297.

Icardi, M., Gavi, E., Marchisio, D. L., Olsen, M. G., Fox, R. O. and Lakehal, D., 2011. Validation of LES predictions for turbulent flow in a confined impinging jets reactor, *Appl. Math. Model*., **35**(4): 1591−1602.

Kiger, K. T. and Duncan, J. H., 2012. Air-entrainment mechanisms in plunging jets and breaking waves, *Annu. Rev. Fluid Mech*., **44**(1): 563−596.

Kim, J. and Moin, P., 1985. Application of a fractional-step method to incompressible Navier-Stokes equations, *J. Comput. Phys*., **59**(2): 308−323.

Lakehal, D. and Liovic, P., 2011. Turbulence structure and interaction with steep breaking waves, *J. Fluid Mech*., **674**, 522−577.

Lubin, P., Vincent, S., Abadie, S. and Caltagirone, J. P., 2006. Three-dimensional large eddy simulation of air entrainment under plunging breaking waves, *Coast. Eng*., **53**(8): 631−655.

Melville, W. K., 1996. The role of surface-wave breaking in air-sea interaction, *Annu. Rev. Fluid Mech.*, **28**(1): 279−321.

Mittal, R. and Iaccarino, G., 2005. Immersed boundary methods, *Annu. Rev. Fluid Mech.*, **37**, 239−261.

Nielsen, P., 1992. *Coastal Bottom Boundary Layers and Sediment Transport*, World Scientific, Singapore.

Sun, D. L. and Tao, W. Q., 2010. A coupled volume-of-fluid and level set (VOSET) method for computing incompressible two-phase flows, *Int. J. Heat Mass Trans.*, **53**(4): 645−655.

Sussman, M., 2003. A second order coupled level set and volume-of-fluid method for computing growth and collapse of vapor bubbles, *J. Comput. Phys.*, **187**(1): 110−136.

Sussman, M. and Puckett, E. G., 2000. A Coupled level set and volume-of-fluid method for computing 3D and axisymmetric incompressible two-phase flows, *J. Comput. Phys.*, **162**(2): 301−337.

Sussman, M., Smereka, P., and Osher, S., 1994. A level set approach for computing solutions to incompressible two-phase flow, *J. Comput. Phys.*, **114**(1): 146−159.

van Rijn, L. C., 1984. Sediment pick-up functions, *J. Hydraul. Eng.*, ASCE, **110**(10): 1494−1502.

Wu, W. M., Rodi, W. and Wenka, T., 2000. 3D numerical modeling of flow and sediment transport in open channels, *J. Hydraul. Eng.*, ASCE, **126**(1): 4−15.

Yakhot, V. and Orszag, S. A., 1986. Renormalization group analysis of turbulence I. Basic theory, *J. Sci. Comput.*, **1**(1): 3−51.

Zedler, E. A. and Street, R. L., 2001. Large-eddy simulation of sediment transport: currents over ripples, *J. Hydraul. Eng.*, ASCE, **127**(6): 444−452.

Zedler, E. A. and Street, R. L., 2006. Sediment transport over ripples in oscillatory flow, *J. Hydraul. Eng.*, ASCE, **132**(2): 180−193.

Zeng, J., Constantinescu, G. and Weber, L., 2008. A 3D non-hydrostatic model to predict flow and sediment transport in loose-bed channel bends, *J. Hydraul. Res.*, **46**(3): 356−372.

Zhang, Z. S., Cui, G. X. and Xu, C. X., 2005. *Theory and Modeling of Turbulence*, Tsinghua University Press, Beijing. (in Chinese)

Zhou, Z. L. and Yan, Y. X., 2009. *Coastal Hydrodynamics*, China Communications Press, Beijing. (in Chinese)

Zhu, J., 1991. A low-diffusive and oscillation-free convection scheme, *Commun. Appl. Numer. Method.*, **7**(3): 225−232.